HHS Public Access

Author manuscript

J Urol. Author manuscript; available in PMC 2017 April 01.

Published in final edited form as:

J Urol. 2016 April ; 195(4 Pt 1): 1110–1117. doi:10.1016/j.juro.2015.10.182.

Intraoperative Optical Biopsy During Robotic-Assisted Radical Prostatectomy Using Confocal Endomicroscopy

Aristeo Lopez[#1,2], **Dimitar V. Zlatev**[#1,2], **Kathleen E. Mach**[1,2], **Daniel Bui**[1,2], **Jen-Jane Liu**[1,2], **Robert V. Rouse**[2,3], **Theodore Harris**[2], **John T. Leppert**[1,2], and **Joseph C. Liao**[1,2,*]

[1] Department of Urology, Stanford University School of Medicine, Stanford, CA 94305-5118

[2] Veterans Affairs Palo Alto Health Care System, Palo Alto, CA 94304

[3] Department of Pathology, Stanford University School of Medicine, Stanford, CA 94305

[#] These authors contributed equally to this work.

Abstract

Purpose—Intraoperative optical biopsy technologies may aid identification of important anatomic landmarks and improve surgical outcomes of robotic-assisted radical prostatectomy (RARP).We sought to evaluate the feasibility of confocal laser endomicroscopy (CLE) during RARP.

Materials and Methods—Twenty-one patients with biopsy-proven prostate cancer scheduled for RARP were recruited. After intravenous administration of fluorescein, 15 patients underwent *in vivo* intraoperative CLE of prostatic and periprostatic structures using either a 2.6-mm or 0.85-mm imaging probe. Standard robotic instruments were used to grasp and maneuver the CLE probes for image acquisition. CLE imaging was performed *ex vivo* on fresh prostate specimens from 20 patients. Confocal video sequences acquired *in vivo* and *ex vivo* were reviewed and analyzed, with additional image processing using a mosaicing algorithm. Processed confocal images were compared with standard hematoxylin and eosin analysis of imaged regions.

Results—CLE was successfully integrated with robotic surgery, including co-registration of confocal video sequences with white light and probe handling with standard robotic instrumentation. Intraoperative CLE imaging of the neurovascular bundle prior to and following nerve-sparing dissection revealed characteristic features including dynamic vascular flow and intact axon fibers. *Ex vivo* confocal imaging of the prostatic parenchyma demonstrated the normal prostatic glands, stroma, and prostate carcinoma.

Conclusions—We report the initial feasibility of optical biopsy of prostatic and periprostatic tissue during RARP. Image guidance and tissue interrogation using CLE offers a new

[*] Corresponding author: Joseph C. Liao, MD, 300 Pasteur Dr., Room S-287, Stanford, CA 94305-5118, jliao@stanford.edu, Phone: 650-858-3916, Fax: 650-849-0319.

intraoperative imaging method that has the potential to improve the functional and oncologic outcomes of prostate cancer surgery.

Keywords

prostatic neoplasms; prostatectomy; microscopy; confocal; erectile dysfunction; surgery; computer-assisted

INTRODUCTION

Cancer control and recovery of urinary and sexual function after radical prostatectomy are related to surgical quality.[1] Since Walsh's initial description of anatomic radical prostatectomy[2], there have been efforts to better understand pelvic anatomy to refine surgical technique. Robotic-assisted radical prostatectomy (RARP) is currently the most common surgical treatment for localized prostate cancer in the United States.[3] Technological advances of the robotic platform include a magnified field of view, tremor filtration, and improved surgeon ergonomics.[4, 5] Despite advances in understanding pelvic anatomy and surgical technologies, there remain significant variations in surgical outcomes of radical prostatectomy, including positive surgical margins (range 6.5% to 32%)[6] and erectile dysfunction (range 7% to 80%).[7, 8]

Image-guided surgery may improve intraoperative navigation and surgical outcomes. Optical imaging technologies offer excellent spatial and temporal resolution, are easily integrated into the operating room, and can be manipulated with instruments commonly used in minimally invasive surgery.[9] For radical prostatectomy, *in vivo* and *ex vivo* feasibility studies have been reported using near-infrared fluorescence imaging [10], optical coherence tomography (OCT)[11-13], and multiphoton microscopy (MPM).[14, 15]

Similar to OCT and MPM, confocal laser endomicroscopy (CLE) is an optical biopsy technology that aims to provide on-demand, high-resolution imaging reminiscent of standard histopathology.[16] CLE is approved for endoscopic applications in gastroenterology, pulmonology, and urology. CLE is based on a 488 nm laser in conjunction with fluorescein, a FDA-approved fluorophore with a demonstrated safety record.[17] We have demonstrated cystoscopic application of CLE for optical diagnosis and grading of bladder cancer[18, 19], as well as *in vivo* visualization of glandular structures within the prostatic urethra.[20] Here, we assess the feasibility of intraoperative CLE during RARP and evaluate potential clinical applications. We developed an intraoperative confocal imaging protocol, characterized *in vivo* microscopic features of prostatic and periprostatic anatomy and compared *ex vivo* imaging of fresh surgical prostate specimens to histopathology.

MATERIAL AND METHODS

Instrumentation

Confocal endomicroscopy was performed with Cellvizio (Mauna Kea Technologies, Paris, France). 2.6-mm or a 0.85-mm outer diameter fiberoptic probes were used for image acquisition (Figure 1A). The 2.6-mm probe has spatial resolution of 1 μm, depth of tissue penetration of 60 μm, and field of view (FOV) of 240 μm. The 0.85-mm probe has spatial

resolution of 3.5 μm, depth of penetration of 50 μm, and a FOV of 320 μm. Probes were sterilized before use with the Sterrad system (Advanced Sterilization Products, Irvine, California).

Intraoperative confocal endomicroscopy during robotic-assisted surgery

The study was conducted with Stanford University Institutional Review Board and Veterans Affairs Palo Alto Health Care System Research and Development Committee approval. Patients with clinically localized prostate cancer scheduled for RARP were recruited. Two surgeons (JCL and JTL) performed the operations and image acquisition. Standard five-port placement consisting of a 12-mm camera port, three 8-mm robotic ports and a 12-mm assistant port was applied. The decision for nerve-sparing was based on clinical staging, technical feasibility, and surgeon discretion. The majority of CLE imaging was performed with a 2.6-mm probe introduced through the 12-mm assistant port (Figure 1B). The robotic needle driver was used to grasp the distal metal tip for imaging (Figure 1C). For the 0.85-mm probe, three strategies were compared for intracorporeal maneuvering: 1) probe insertion via a standard laparoscopic cholangiogram catheter holder operated by bedside assistant, 2) probe insertion via a 5 French angiocatheter through assistant port and grasping using the robotic needle driver; and 3) probe insertion via a 19-gauge angiocatheter introduced suprapubically as a needlescopic port and grasping using the robotic needle driver (Figure 1D).

Approximately 5 minutes prior to dissection of the neurovascular bundle (NVB), 2.5 ml 10% sodium fluorescein (Akorn, Lake Forest, IL) was administered intravenously. For imaging, the probe tip was positioned perpendicular to the tissue for *en face* contact and rinsed with irrigation as needed to remove blood or debris. Images were acquired as video sequences at 12 frames per second. TilePro (Intuitive Surgical, Sunnyvale, CA) was used to simultaneously view the white light stereoscopic view of the operative field and confocal imaging (Figure 1C-D). Prostatic and periprostatic structures, including levator fascia, NVB before and after nerve-sparing procedure, prostatic capsule, bladder neck, urethral stump, and pelvic floor, were imaged *in situ*, reviewed in real-time, and recorded for additional offline analysis.

Ex vivo confocal endomicroscopy of prostate specimens

Ex vivo CLE was performed within 1 hour of specimen retrieval. To optimize prostatic parenchymal staining, an additional 2.5 ml of 10% fluorescein was administered intravenously before the division of the prostatic pedicles. CLE image acquisition was performed by manual manipulation of the 2.6-mm probe. Imaged regions on the surface of the prostate included the prostatic capsule, posterolateral surface corresponding to the location of the NVB, and apical margins. To characterize parenchymal structures, the prostate was sectioned transversely with the assistance of a surgical pathologist (RVR). Each 5 mm thick prostate slice was divided into quadrants and systematically imaged in a defined pattern. Additional fluorescein was applied topically (2 minute incubation then 7 minute saline wash to remove excess fluorescein) to enhance visualization. After imaging, tissues were fixed in formalin and sent for hematoxylin and eosin (H&E) staining and

histopathologic analysis. Immunohistochemistry against S100 proteins was performed on select sections (HistoTec, Hayward, CA) to identify nerves.

Data analysis

In vivo and *ex vivo* confocal video sequences were reviewed, edited, and analyzed offline using Cellvizio Viewer v1.6 software. A built-in mosaicing algorithm was used to compile consecutive images into a single larger composite image. Processed confocal images were compared with corresponding H&E stains and reviewed with a surgical pathologist (RVR).

RESULTS

Between December 2012 and March 2015, 21 patients (mean age 62 years, range 49 to 69) scheduled for RARP at VAPAHCS were recruited. Patients underwent either bilateral (n=16) or unilateral nerve-sparing (n=5) RARP. *In vivo* CLE imaging was performed in 15 patients and *ex vivo* imaging was performed on 20 prostates. Patient characteristics and imaging details are described in Table 1.

105 *in vivo* confocal video sequences from 15 patients were collected. The average image acquisition time was 10 min (range 3 to 18 min) per participant. An average of 7 video sequences (range 4 to 12 sequences) were obtained per case. The average duration of imaging at each area was 91 seconds (range 6 to 303 seconds). In one patient, the metal tip of the 2.6-mm probe broke off during handling by the robotic instrument and was removed with a laparoscopic grasper without complication. There were no adverse events related to fluorescein administration.

Comparison of the 2.6-mm and 0.85-mm imaging probes

We compared intraoperative handling and image quality of 2.6-mm and 0.85-mm probes. The 2.6-mm and 0.85-mm probes were tested in 11 and 4 participants, respectively. The 2.6-mm probe was previously validated for bladder cancer imaging. The 0.85-mm probe was described for CLE of pancreatic cysts through a 19-gauge biopsy needle [21] and upper urinary tract through standard ureteroscopes.[22] The smaller 0.85 mm probe has potential for greater flexibility for intraoperative probe deployment. While inserted through the 12-mm assistant port, both probes were compatible with in-parallel insertion of additional instruments without significant loss of pneumoperitoneum. To minimize trauma to optical fibers, the 2.6-mm probe was handled by grasping the distal metal tip (Figure 1C), whereas the 0.85 mm probe was inserted via a laparosopic cholangiogram instrument (n=1), 5 French catheter (n=2), or a 19 gauge angiocatheter for maneuvering with the robotic needle holder (n=1, Figure 1D). Overall, the flexibility of the fiberoptic probes enabled efficient access to various pelvic anatomic landmarks for imaging. Given its higher spatial resolution, the image quality from the 2.6-mm probe was significantly better than the 0.85-mm probe, therefore the 2.6-mm probe was used exclusively after the fourth case (Table 1). The image quality of the probes did not noticeably diminish with repeated sterilization.

Neurovascular bundle imaging

Prior *ex vivo* studies indicate that NVBs are located posterolaterally of the prostate and enclosed in lateral pelvic fascia.[23, 24] Intraoperative CLE of regions corresponding to the NVB was performed before and after nerve-sparing dissection. Characteristic confocal features of the NVB include parallel thin dark lines corresponding to axonal fibers, bordered by dark cells consistent with adipocytes, and interspersed with vessels with flowing erythrocytes (Figure 2, Supplementary Movie S1). Generally, confocal features of NVBs were not visualized until the lateral pelvic fascia was incised. NVBs were visualized with both the 0.85-mm (Figure 2A) and 2.6-mm imaging probes (Figure 2B-E). The mosaicing algorithm was applied offline to generate a wide-field view of the NVB (Figure 2G). *In vivo* CLE identified the NVB in 11 of 15 patients. In one case, residual nerve tissues were observed on the prostatic capsule following initial dissection, prompting additional dissection and CLE confirmation of NVB separation from prostate.

Identification of prostatic and periprostatic structures

Representative *in vivo* confocal images of prostatic and periprostatic structures are shown in Figure 3. The prostatic capsule (Figure 3A), bladder neck margin (Figure 3B), urethral stump, levator ani (Figure 3C), and obturator nerve (Figure 3D) were imaged. Imaging of the prostatic capsule demonstrated striated fibrous tissue with occasional small caliber vasculature. Given the relatively small FOV of CLE, the prostatic capsule was not comprehensively imaged *in vivo*. No discernible prostatic parenchymal features such as glandular structures were observed *in vivo*. Confocal imaging of the bladder neck mucosa showed normal urothelium with umbrella and intermediate cells and the underlying vasculature of the lamina propria, consistent with previous bladder imaging.[20]

Ex vivo confocal imaging of fresh prostate tissue

To further characterize the confocal imaging features with H&E correlation, fresh prostate specimens were imaged *ex vivo*. A total of 259 imaging sequences were collected from 20 subjects. The prostate was imaged intact (Figure 4A) to visualize the capsular features, followed by imaging of prostate sections to visualize the parenchymal structures (Figure 4B). In patients with non-nerve-sparing procedure, residual NVBs were observed on the prostate specimen (Figure 2E) and confirmed by H&E and immunohistochemistry staining of myelin-specific antigen S100 (Supplementary Figure S1). While most prostate cancer arises from the peripheral zone[25], given the 60-μm depth of penetration of CLE, we did not expect to visualize stromal and glandular structures through an intact capsule unless were positive surgical margins or extracapsular extension (ECE). In specimen #7 (Table 1) with pT3B disease, CLE imaging along the lateral prostatic capsule showed glandular structures distinct from the surrounding fibrous capsule (Figure 4C). This patient was confirmed to have multifocal ECE on pathology. On prostate sections, benign prostatic glands were characterized by lobular structures with a rim of increased surrounding fluorescence (Figure 4E). Benign features such as corpora amylacea were easily identified as round circumscribed structures within glands (Figure 4G). Prostatic glands in tissues found to contain carcinoma were characterized by smaller, less regular lobular structures without a surrounding rim of fluorescence (Figure 4I).

DISCUSSION

We report the initial feasibility of *in vivo* CLE during RARP. We demonstrated ease of integrating CLE with robotic surgery, including co-registration of confocal video sequences with white light imaging, probe handling with standard robotic instrumentation, and tremor-free image acquisition. We characterized *in vivo* imaging features of clinically relevant prostatic and periprostatic anatomic landmarks, particularly the NVB. Intraoperative CLE was performed successfully with 2.6-mm and 0.85-mm probes, with the 2.6-mm probe offering superior image quality. Dynamic imaging of intact NVBs demonstrated parallel axonal fibers lined by adipocytes and small caliber vessels. *In vivo* microscopy features of the NVB were confirmed with *ex vivo* CLE and standard H&E in prostate samples where nerve-sparing was not performed.

Erectile dysfunction is a complication of radical prostatectomy that can be minimized by preservation of the NVB. Since components of the NVB have variable distribution and location[23] and cannot be visualized directly during surgery, nerve-sparing techniques are based on gross inspection and minimization of thermal energy use near the presumed NVB location. Intraoperative visualization of microscopic features may better guide nerve-sparing surgery and provide real-time feedback for adequate dissection. Our results suggest that CLE may be used to map NVB location. Dynamic characterization of the intact NVB after dissection may serve as a marker of successful preservation of the NVB.

Positive surgical margin status is an adverse oncologic outcome of radical prostatectomy that might be improved by image-guided identification of ECE at surgical margins. *Ex vivo* CLE of prostatic sections revealed benign and cancerous glandular structures. While most of the patients in this series had organ-confined disease, in the cases of pT3b disease we were able to detect apparent ECE of carcinoma. CLE could be utilized in conjunction with preoperative magnetic resonance imaging for targeted intraoperative imaging of areas concerning for ECE. Identification of any glandular structures at surgical margins would prompt the surgeon to redirect the plane of dissection.

CLE differs from other optical biopsy technologies. Compared to clinical OCT systems,[11, 12] CLE offers a higher spatial resolution but lower depth of penetration. MPM offers spatial resolution similar to CLE and improved depth of penetration, however current studies using MPM are limited to *ex vivo* human specimens and *in vivo* animal studies.[14, 15] While OCT and MPM do not require the administration of exogenous dye, fluorescein is inexpensive, has a proven safety profile,[17] and may be coupled with targeting agents for molecular imaging using CLE to further improve optical diagnostics. [26, 27]

The small sample size and pilot nature of this study precluded diagnostic accuracy assessment of CLE imaging of the prostate. Furthermore, the impact that CLE may have on long-term functional outcomes is unknown, as CLE was not used to direct surgical guidance. A larger sample size and defined clinical endpoints will be necessary to assess the clinical benefits of CLE during RARP. Visualization of intact nerves does not equate to functional nerves. Future integration of CLE with molecular imaging agents[28] or nerve stimulator[29] may provide physiological feedback of nerve function. Other technical limitations include

the small FOV of CLE, which makes intraoperative surveying of large surface areas impractical. This may not negatively impact the utility of CLE for nerve-sparing procedures as it was possible to scan the length of the NVB within 90 seconds, but may limit use of CLE for detection of incidental ECE. While CLE imaging is optimal within 20 minutes of fluorescein administration, we demonstrated the feasibility of fluorescein re-dosing. Future investigation of topical contrast administration with an endoscopic spray catheter [30] may offer alternative strategies for intraoperative CLE without the requirement of intravenous fluorescein.

CLE is a promising technology for microscopic imaging during RARP. CLE optical biopsy of live tissue may provide a new method for intraoperative identification of NVB with spatial and temporal resolutions previously not described. Additional experience is required to assess the utility of CLE to detect surgical margin status and to evaluate if this promising imaging technique will translate to improved oncologic and functional outcomes.

CONCLUSIONS

CLE of prostate and NVB is feasible during RARP. Nerve fibers can be visualized and differentiated from vessels and connective tissue. *Ex vivo* CLE can be used to identify prostatic glandular structures and ECE. Additional prospective analysis is required to assess the clinical benefits of CLE-guided nerve-sparing RARP.

Supplementary Material

Refer to Web version on PubMed Central for supplementary material.

ACKNOWLEDGEMENTS

This work was supported by in part by U.S. National Institute of Health R01 CA160986 to JCL.

KEY OF DEFINITIONS FOR ABBREVIATIONS

CLE	confocal laser endomicroscopy
ECE	extracapsular extension
FOV	field of view
H&E	hematoxylin and eosin3
MPM	multiphoton microscopy
NVB	neurovascular bundle
OCT	optical coherence tomography
RARP	robotic-assisted radical prostatectomy

REFERENCES

1. Vickers A, Savage C, Bianco F, et al. Cancer control and functional outcomes after radical prostatectomy as markers of surgical quality: analysis of heterogeneity between surgeons at a single cancer center. Eur Urol. 2011; 59:317. [PubMed: 21095055]
2. Walsh PC. Anatomic radical prostatectomy: evolution of the surgical technique. J Urol. 1998; 160:2418. [PubMed: 9817395]
3. Tsui C, Klein R, Garabrant M. Minimally invasive surgery: national trends in adoption and future directions for hospital strategy. Surg Endosc. 2013; 27:2253. [PubMed: 23660720]
4. Sood A, Jeong W, Peabody JO, et al. Robot-assisted radical prostatectomy: inching toward gold standard. Urol Clin North Am. 2014; 41:473. [PubMed: 25306159]
5. Volonte F, Pugin F, Buchs NC, et al. Console-integrated stereoscopic OsiriX 3D volume-rendered images for da Vinci colorectal robotic surgery. Surg Innov. 2013; 20:158. [PubMed: 22549904]
6. Yossepowitch O, Briganti A, Eastham JA, et al. Positive surgical margins after radical prostatectomy: a systematic review and contemporary update. Eur Urol. 2014; 65:303. [PubMed: 23932439]
7. Alemozaffar M, Regan MM, Cooperberg MR, et al. Prediction of erectile function following treatment for prostate cancer. JAMA. 2011; 306:1205. [PubMed: 21934053]
8. Johansson E, Bill-Axelson A, Holmberg L, et al. Time, symptom burden, androgen deprivation, and self-assessed quality of life after radical prostatectomy or watchful waiting: the Randomized Scandinavian Prostate Cancer Group Study Number 4 (SPCG-4) clinical trial. Eur Urol. 2009; 55:422. [PubMed: 18783877]
9. Hsu M, Gupta M, Su LM, et al. Intraoperative optical imaging and tissue interrogation during urologic surgery. Curr Opin Urol. 2014; 24:66. [PubMed: 24240512]
10. KleinJan GH, van den Berg NS, Brouwer OR, et al. Optimisation of fluorescence guidance during robot-assisted laparoscopic sentinel node biopsy for prostate cancer. Eur Urol. 2014; 66:991. [PubMed: 25092539]
11. Aron M, Kaouk JH, Hegarty NJ, et al. Second prize: preliminary experience with the Niris optical coherence tomography system during laparoscopic and robotic prostatectomy. J Endourol. 2007; 21:814. [PubMed: 17867934]
12. Muller BG, de Bruin DM, van den Bos W, et al. Prostate cancer diagnosis: the feasibility of needle-based optical coherence tomography. J Med Imaging (Bellingham). 2015; 2:037501. [PubMed: 26171414]
13. Rais-Bahrami S, Levinson AW, Fried NM, et al. Optical coherence tomography of cavernous nerves: a step toward real-time intraoperative imaging during nerve-sparing radical prostatectomy. Urology. 2008; 72:198. [PubMed: 18280549]
14. Durand M, Jain M, Aggarwal A, et al. Real-time in vivo periprostatic nerve tracking using multiphoton microscopy in a rat survival surgery model: a promising pre-clinical study for enhanced nerve-sparing surgery. BJU Int. 2014
15. Tewari AK, Shevchuk MM, Sterling J, et al. Multiphoton microscopy for structure identification in human prostate and periprostatic tissue: implications in prostate cancer surgery. BJU Int. 2011; 108:1421. [PubMed: 21443651]
16. Chen SP, Liao JC. Confocal laser endomicroscopy of bladder and upper tract urothelial carcinoma: a new era of optical diagnosis? Curr Urol Rep. 2014; 15:437. [PubMed: 25002073]
17. Wallace MB, Meining A, Canto MI, et al. The safety of intravenous fluorescein for confocal laser endomicroscopy in the gastrointestinal tract. Aliment Pharmacol Ther. 2010; 31:548. [PubMed: 20002025]
18. Chang TC, Liu JJ, Liao JC. Probe-based confocal laser endomicroscopy of the urinary tract: the technique. J Vis Exp. 2013:e4409. [PubMed: 23354133]
19. Sonn GA, Jones SN, Tarin TV, et al. Optical biopsy of human bladder neoplasia with in vivo confocal laser endomicroscopy. J Urol. 2009; 182:1299. [PubMed: 19683270]
20. Wu K, Liu JJ, Adams W, et al. Dynamic real-time microscopy of the urinary tract using confocal laser endomicroscopy. Urology. 2011; 78:225. [PubMed: 21601243]

21. Konda VJ, Meining A, Jamil LH, et al. A pilot study of in vivo identification of pancreatic cystic neoplasms with needle-based confocal laser endomicroscopy under endosonographic guidance. Endoscopy. 2013; 45:1006. [PubMed: 24163192]
22. Bui D, Mach KE, Zlatev DV, et al. A Pilot Study of In Vivo Confocal Laser Endomicroscopy of Upper Tract Urothelial Carcinoma. J Endourol. Oct 6.2015 [Epub ahead of print].
23. Kiyoshima K, Yokomizo A, Yoshida T, et al. Anatomical features of periprostatic tissue and its surroundings: a histological analysis of 79 radical retropubic prostatectomy specimens. Jpn J Clin Oncol. 2004; 34:463. [PubMed: 15371464]
24. Tewari AK, Srivastava A, Huang MW, et al. Anatomical grades of nerve sparing: a risk-stratified approach to neural-hammock sparing during robot-assisted radical prostatectomy (RARP). BJU Int. 2011; 108:984. [PubMed: 21917101]
25. McNeal JE, Redwine EA, Freiha FS, et al. Zonal distribution of prostatic adenocarcinoma. Correlation with histologic pattern and direction of spread. Am J Surg Pathol. 1988; 12:897. [PubMed: 3202246]
26. Nguyen QT, Tsien RY. Fluorescence-guided surgery with live molecular navigation--a new cutting edge. Nat Rev Cancer. 2013; 13:653. [PubMed: 23924645]
27. Pan Y, Volkmer JP, Mach KE, et al. Endoscopic molecular imaging of human bladder cancer using a CD47 antibody. Sci Transl Med. 2014; 6:260ra148.
28. Boyette LB, Reardon MA, Mirelman AJ, et al. Fiberoptic imaging of cavernous nerves in vivo. J Urol. 2007; 178:2694. [PubMed: 17945279]
29. Burnett AL, Teloken PE, Briganti A, et al. Intraoperative assessment of an implantable electrode array for cavernous nerve stimulation. J Sex Med. 2008; 5:1949. [PubMed: 18466264]
30. Hsiung PL, Hardy J, Friedland S, et al. Detection of colonic dysplasia in vivo using a targeted heptapeptide and confocal microendoscopy. Nat Med. 2008; 14:454. [PubMed: 18345013]

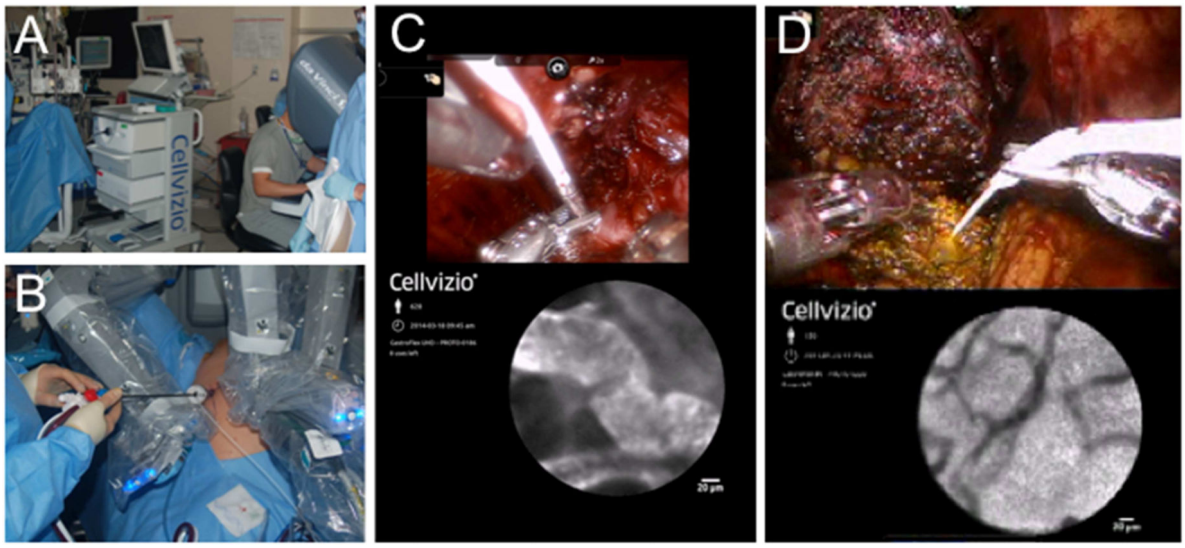

Figure 1. Intraoperative CLE during robotic prostatectomy

(A) CLE tower arrangement at the head of the operating room table. (B) 2.6-mm imaging probe inserted through a 12-mm laparoscopic port alongside a suction-irrigator. (C) Confocal imaging of the neurovascular bundle with the 2.6-mm imaging probe held by a robotic needle driver. TilePro functionality enabled simultaneous display of the confocal image and white light stereoscopic view of the operative field within the surgeon console. (D) Confocal imaging of the divided bladder neck using the 0.85-mm probe inserted through a 19-gauge angiocatheter. The confocal image shows vasculature of the bladder lamina propia.

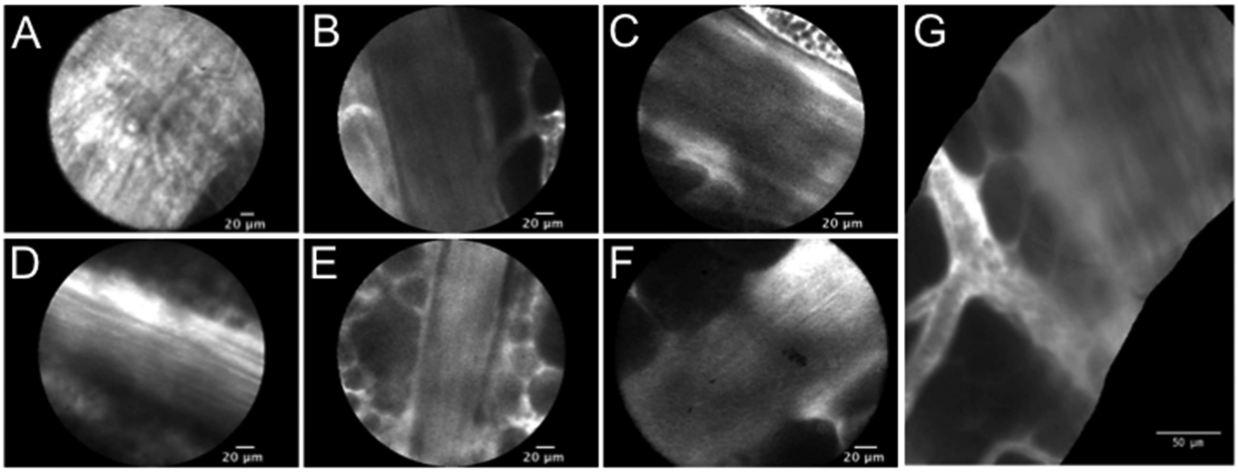

Figure 2. CLE images of the neurovascular bundle (NVB)

Nerve axons visualized with (A) the 0.85-mm probe and (B-G) the 2.6-mm probe. Nerves were visualized (B) prior to and (C-D) after NVB dissection. (E) Residual nerve structures present on the prostate capsule after neurovascular dissection. (F) Intact NVB seen *ex vivo* on a non-sparing prostate specimen. (G) Panoramic image of NVB generated with mosaicing algorithm from images obtained during *in vivo* CLE, with erythrocytes within blood vessels on the left and nerve fibers on the right.

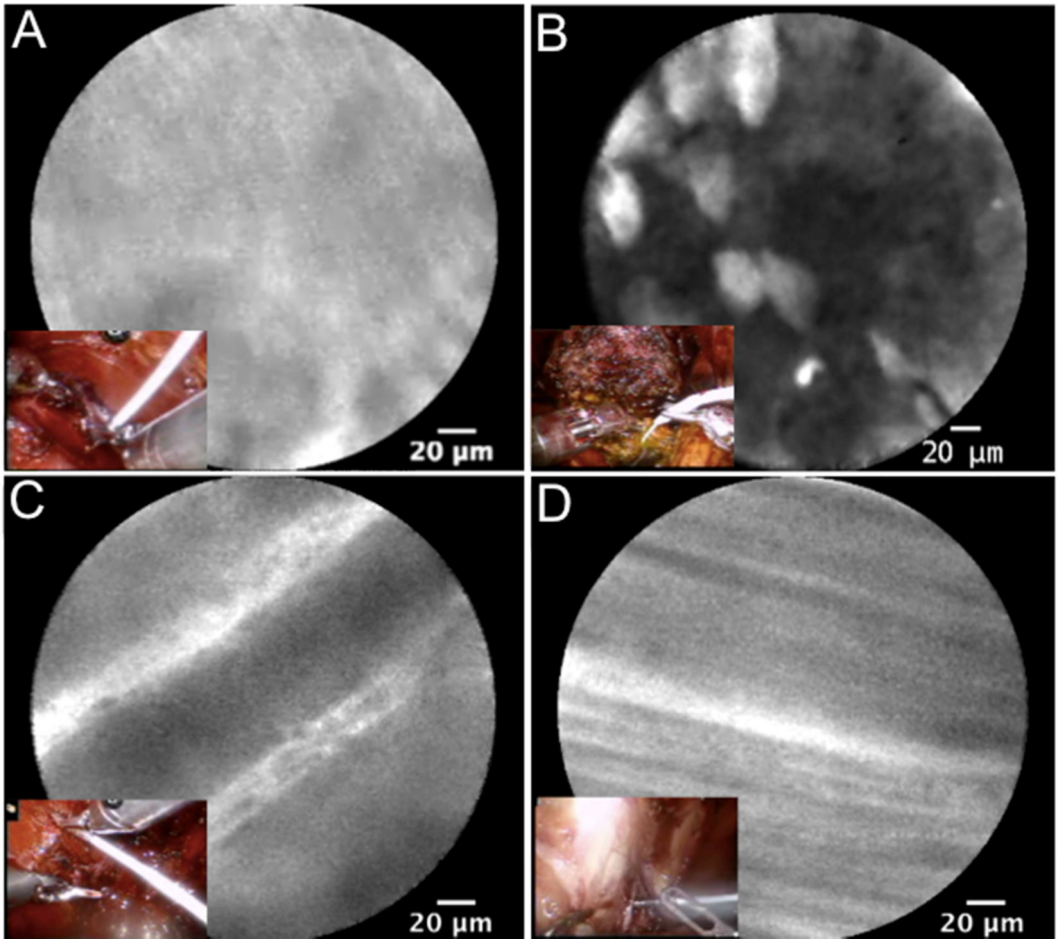

Figure 3. ***In vivo*** **CLE of prostatic and periprostatic structures, with corresponding stereoscopic views from robotic prostatectomy as insets**

Confocal characteristics of the (A) fibrous prostatic capsule, (B) urothelium of the bladder neck margin, (C) levator ani muscle fibers, and (D) axons of the obturator nerve.

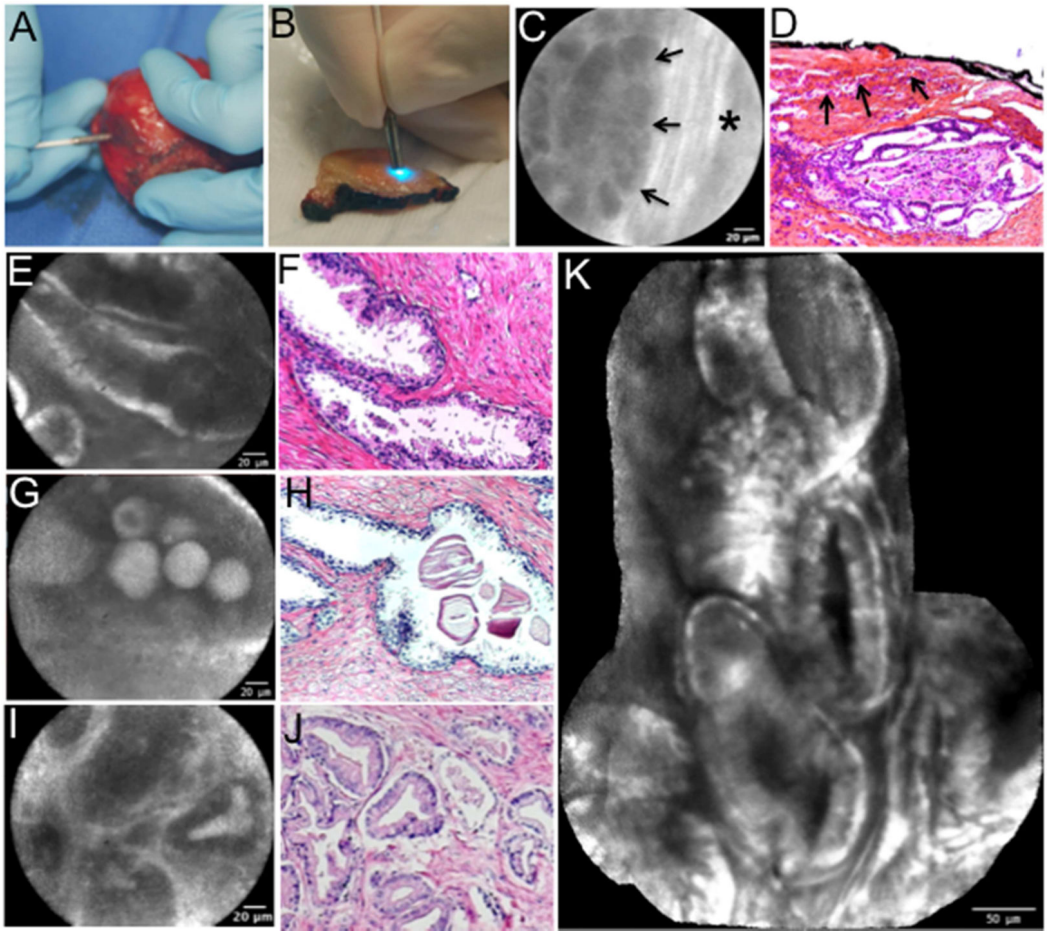

Figure 4. ***Ex vivo*** **CLE imaging of prostatic tissue with corresponding hematoxylin and eosin (H&E)**

(A) CLE probe application to intact prostate specimen. (B) CLE probe application to transverse cut section of prostate. (C,D) Extra capsular extension of carcinoma, arrows point to region of ECE in background of striated pattern capsule marked by * with corresponding H&E at 50× magnification (E, F) Lobular structure of benign prostatic glands. (G, H) Corpora amylacea within glands. (I, J) Prostate cancer glands with a Gleason 3+3 pattern. Corresponding H&E for F, H and J at 100X magnification. (K) Panoramic image of normal prostate generated with a mosaicing algorithm that increased the field of view by approximately 4-fold.

Table 1

Patient characteristics, confocal endomicroscopy, and histopathological diagnoses.

Prostate	Age	CLE Probe	In Vivo Imaging	Ex Vivo Imaging	Nerve Sparing	Gleason Score	Stage	ECE*
1	49	0.85-mm	Y	Y	Bilateral	3+3, tertiary 4	pT2c Nx	None
2	57	0.85-mm	Y	Y	Bilateral	3+4	pT3a N0	Focal
3	65	0.85-mm	Y	Y	Bilateral	3+3	pT2a N0	None
4	57	0.85-mm	Y	Y	Bilateral	3+4	pT2a N0	None
5	70	2.6-mm	N	Y	Bilateral	3+4	pT2c N0	None
6	64	2.6-mm	Y	Y	Bilateral	3+4	pT2c N0	None
7	64	2.6-mm	Y	Y	Bilateral	3+4	pT3b N0	Present
8	66	2.6-mm	N	Y	Unilateral, right	4+3	pT2c N0	None
9	65	2.6-mm	N	Y	Bilateral	4+3	pT3b N0	Focal
10	53	2.6-mm	Y	Y	Unilateral, right	3+4	pT3a N0	Focal
11	57	2.6-mm	N	Y	Unilateral, left	4+5	pT3a N0	Focal
12	52	2.6-mm	Y	Y	Bilateral	3+3, tertiary 4	pT2c N0	None
13	63	2.6-mm	Y	Y	Bilateral	3+4	pT2b Nx	None
14	66	2.6-mm	Y	Y	Bilateral	3+3	pT2b N0	None
15	67	2.6-mm	Y	Y	Bilateral	3+4	pT2c N0	None
16	65	2.6-mm	Y	Y	Unilateral, left	4+3	pT2a N0	None
17	65	2.6-mm	N	Y	Bilateral	4+4	pT3a N0	Present
18	69	2.6-mm	Y	Y	Unilateral, right	4+4	pT2a N0	None
19	59	2.6-mm	N	Y	Bilateral	3+3	pT2c N0	None
20	65	2.6-mm	Y	Y	Bilateral	3+3, tertiary 4	pT2c Nx	None
21	67	2.6-mm	Y	N	Bilateral	3+4	pT2a N0	None

CLE, confocal laser endomicroscopy.

*Extra capsular extension